A Cascaded Power Controller for Robust Frequency Ride-Through of Grid-Forming Converters

A Cascaded Power Controller for Robust Frequency Ride-Through of Grid-Forming Converters

Paul Imgart
Division of Electric Power Engineering
Chalmers University of Technology
Göteborg, Sweden
paul.imgart@chalmers.se

Anant Narula
Division of Electric Power Engineering
Chalmers University of Technology
Göteborg, Sweden
anant.narula@chalmers.se

Massimo Bongiorno
Division of Electric Power Engineering
Chalmers University of Technology
Göteborg, Sweden
massimo.bongiorno@chalmers.se

Mebtu Beza
Division of Electric Power Engineering
Chalmers University of Technology
Göteborg, Sweden
mebtu.beza@chalmers.se

Jan R. Svensson
Hitachi Energy Research
Hitachi Energy
Västerås, Sweden
jan.r.svensson@hitachienergy.com

***Abstract*—The aim of this paper is to present a grid-forming (GFM) control strategy with a novel active-power loop (APL) structure facilitating limitation of active power while providing maximum available inertial support. This is achieved by decoupling the synchronization duties of the APL from the inertial support. The latter is provided by calculating an active-power reference through a dedicated inertia-emulation loop (IEL), which is connected in cascade with the APL. The effectiveness of the proposed method is demonstrated through time-domain simulations including frequency transients of varying size and unbalanced operating conditions.**

***Index Terms*—Grid-forming converter, grid-connected converter, inertia, low-inertia power system, frequency stability, rate of change of frequency, current limiting**

I. Introduction

World-wide transformation efforts towards the future renewable-based power system result in the replacement of synchronous with converter-interfaced generation. Thanks to their voltage source behaviour and ability to easily provide a number of ancilliary services such as inertial support, grid-forming (GFM) converters are the preferred solution for the challenges associated with this development [1]. One of the main challenges for GFM converters is to be able to limit the converter current and at the same time maintain a stable operation and GFM properties [2]. In this regard there is a lot of focus in existing studies dealing with converter angle stability and related design improvements on current limitation during voltage dips [3]–[7]. However, as this paper will show, grid frequency disturbance is a relevant source of angular instability; this kind of disturbance is particularly challenging when large inertial support is required and grid synchronization is provided by the active-power loop (APL).

Even though the focus of existing work has been on instability caused by voltage fluctuations, there exist some publications suggesting solutions for frequency-disturbance induced instability. From the existing literature, mainly three strategies have been identified. The first is control-mode switching (CMS), as suggested in [8], where a complex modified droop control manipulates the active and reactive power references based on the converter currents to prevent loss of synchronism due to current saturation. A different approach involving CMS is presented in [9], selecting different frequency response strategies based on frequency deviation and the typically noise-sensitive estimate of the rate of change of frequency (RoCoF). The second strategy is to adapt the inertia, which in [10] is based on a grid impedance estimation to ensure a selected stability margin for the GFM converter. The third strategy is to switch the synchronization duty during current limitation to a backup synchronization unit, typically a phase-locked loop (PLL) [11], [12]. CMS as well as parameter adaptation change the converter's properties abruptly. Some implementations require typically unknown system parameters to properly estimate the converter's actual capabilities and otherwise limit too conservatively or have the risk of not staying within the limits [13]. The use of a backup PLL during current saturation can result in the removal of the converter's GFM capabilities, which is undesirable as they are typically needed the most during grid disturbances. Furthermore, the suggested solutions to the GFM converter stability problem are closely integrated with the rest of the suggested control system, making them highly specific.

The aim of this paper is to propose a solution to the GFM stability problem by decoupling the synchronization task of the APL from the provision of inertia. To address the issue properly, first it is investigated what the root causes of angular instability in GFM converters are and why controllers which provide inertial support are prone to instability when subjected to large grid frequency disturbances. It is shown that existing solutions available in the literature, typically based on variation of the active-power reference [3]–[7], are not effective for

The funding received from Energimyndigheten, Svenska Kraftnät and Hitachi Energy is thankfully acknowledged.

this kind of event. Based on this analysis, a new solution consisting of an inertia-emulation loop (IEL) in cascade with a fast active-power controller is presented. The IEL is based on the structure of a PLL and is used to generate an active-power reference emulating the desired amount of inertia, whereas the APL provides synchronization with the grid. Next, the tuning procedure for APL and IEL is established, demonstrating how the IEL parameters relate to the desired inertia constant and damping ratio of the inertial response. This is followed by results of time-domain simulations, presented to demonstrate that the desired behavior is achieved. Thanks to the proposed control strategy, it is possible to keep the grid-forming properties and the converter current limits without the need for control-mode switching or parameter adaptation.

II. Grid-forming converter stability problem

The common property of the majority of the GFM control structures suggested in the literature is that the converter should be modelled as a voltage source behind an impedance [14], [15]. This behavior can be achieved using different grid-synchronization methods, e.g. using a dedicated synchronization unit like a PLL. However, GFM converters typically synchronize by relying on the active-power transfer, which can even provide increased robustness in weak grids and islanding operation [16]. In this work, the virtual admittance-based approach from [17] is implemented with the structure displayed in Fig. 1. A detailed description of the control system follows in the next section, as the results of this study are not specific for this control structure.

Angle instability in GFM converters mainly occurs due to two reasons: firstly, the power reference being too large for the grid conditions such as grid strength and voltage, e.g. during a fault [3]–[7]; secondly, the power controller being unable to follow the grid voltage angle in case of an angle jump or frequency disturbance. The latter is the focus of this paper.

For the system depicted in Fig. 1 (bottom figure), neglecting the system losses the steady state per-unit converter current is

$$\underline{I}_\mathrm{c} = \frac{\underline{V}_\mathrm{EMF} - \underline{V}_\mathrm{s}}{\mathrm{j}X} = \frac{V_\mathrm{s}\sin\delta + \mathrm{j}(V_\mathrm{s}\cos\delta - V_\mathrm{EMF})}{X}, \quad (1)$$

where the dq-frame is aligned with the converter back EMF, δ denotes the phase displacement between $\underline{V}_\mathrm{EMF}$ and $\underline{V}_\mathrm{s}$, and X is the sum of reactances between them[1]. The active-power transfer from the converter to the grid is defined with $*$ symbolizing the complex conjugate as

$$P = \Re\mathfrak{e}\{\underline{V}_\mathrm{EMF}\underline{I}_\mathrm{c}^*\} = \frac{V_\mathrm{s}V_\mathrm{EMF}}{X}\sin\delta, \quad (2)$$

and shown in blue in Fig. 2 for an example system.

Denoting with I_max the maximum allowed converter current and using circular current limitation [6] on the current reference I_ref, the limited converter current reference is

$$\underline{I}_\mathrm{ref,lim} = \underline{I}_\mathrm{ref}\frac{I_\mathrm{max}}{I_\mathrm{ref}} \qquad \forall\ I_\mathrm{ref} > I_\mathrm{max}. \quad (3)$$

[1]The virtual admittance $\underline{Y}_\mathrm{v} = \underline{Z}_\mathrm{v}^{-1}$ in Fig. 1 is the inverse of the series of the virtual impedance $\underline{Z}_\mathrm{v1}$ and the physical filter impedance $\underline{Z}_\mathrm{f}$.

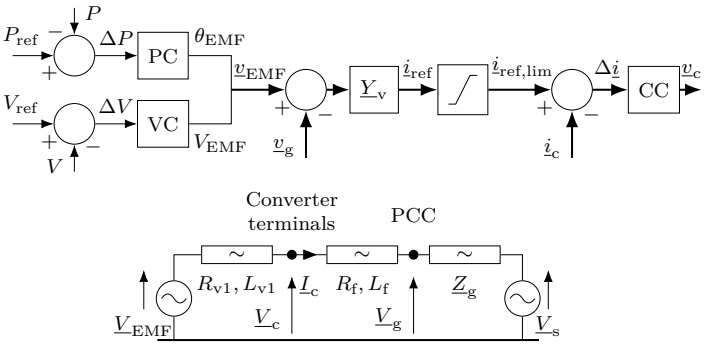

Fig. 1. Block scheme (top) and equivalent circuit (bottom) representation of the virtual admittance-based GFM control approach.

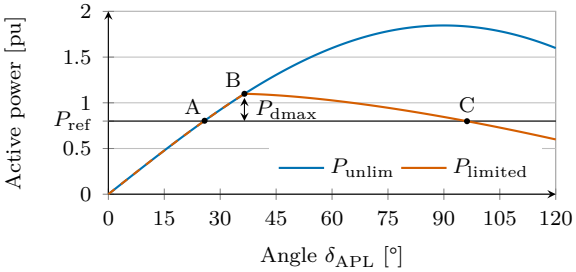

Fig. 2. P-δ_APL curve illustrating the converter angle stability problem for a current limit of 1.1 pu with $V_\mathrm{g} = 1$ pu. A: Pre-disturbance operating point; B: Current limit reached; C: transient stability limit; P_dmax: maximum decelerating power.

Note that the activation of the current limiter is equivalent to a variation of the phasor $\underline{V}_\mathrm{EMF}$, defined as $\underline{V}'_\mathrm{EMF}$ in Fig. 3. From the figure, current limitation results in a reduction of the load angle δ when compared with the unlimited case, denoted as δ_APL. Even despite this reduction, the angle δ_APL still has an impact on the exchanged active power, as it determines the angle of the current reference $\underline{I}_\mathrm{ref}$. Using (1)-(3), the relation between δ_APL and the current-limited active power P_limited is given as

$$\begin{aligned} P_\mathrm{limited} &= \Re\mathfrak{e}\{\underline{V}_\mathrm{s}\underline{I}^*_\mathrm{ref,lim}\} \quad (4)\\ &= V_\mathrm{s}V_\mathrm{EMF}\sin\delta_\mathrm{APL}\frac{I_\mathrm{max}}{\sqrt{V_\mathrm{s}^2 + V_\mathrm{EMF}^2 - 2V_\mathrm{s}V_\mathrm{EMF}\cos\delta_\mathrm{APL}}}, \\ &\qquad \forall\ I_\mathrm{ref} > I_\mathrm{max}. \end{aligned}$$

Figure 2 illustrates the current-limited P-δ_APL relationship following from (4) in red. After the current saturates at B, the power transfer decreases for increasing δ_APL.

The type of instability highlighted in this section occurs due to the inability of the APL to follow the grid voltage angle in case of a severe frequency disturbance or phase angle

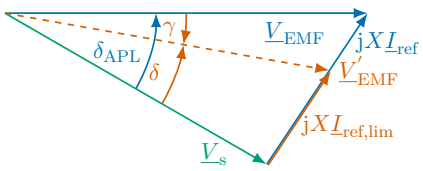

Fig. 3. Phasor diagram illustrating the effect of current limitation on the virtual back EMF. Unlimited in blue, limited in red.

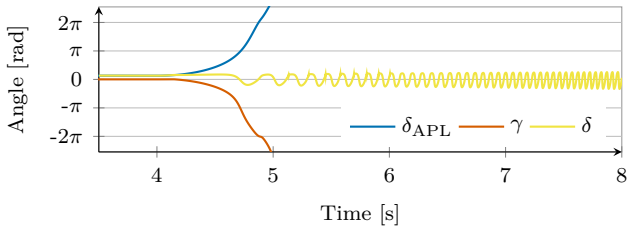

Fig. 4. δ_{APL}, γ and δ for converter instability due to frequency disturbance at 4 s.

jump. To follow a change in the grid frequency, a power control error is required, causing the APL to adapt its internal frequency. As an example, a frequency decline would cause the angle to increase until the additional decelerating power $P_{\mathrm{d}} = -2H\frac{\mathrm{d}\omega}{\mathrm{d}t}$ is achieved. When the current is limited, the needed decelerating power might not be reached and the angle continues to increase. Synchronism is lost if the unstable equilibrium point C is passed, equivalent to synchronous machine first swing instability.

The simulation shown in Fig. 4 illustrates this instability mechanism caused by a frequency decrease. During unsaturated operation, γ defined in Fig. 3 is zero. During limitation, the required deceleration power P_{d} cannot be reached and the APL angle δ_{APL} increases steadily. As a consequence, γ is decreasing at an accelerating rate, which demonstrates the loss of the synchronization signal. In this case, loss of synchronism cannot be prevented by limiting the active-power reference, because the additional power is not caused by a change in reference, but by the slow APL's inability to reject the grid disturbance. GFM converters are prone to this type of instability when they rely on the active power transfer for synchronization. Due to this, the APL output is not a load angle, but a ramp-formed phase angle. When the APL angle output is manipulated to guarantee current limitation, the synchronization signal is lost. Large inertia, high RoCoF and operating points close to the maximum power transfer will increase the risk for this kind of instability, as the necessary decelerating power increases or the available current for decelerating power decreases, respectively.

III. Proposed Solution

The GFM design incorporating both synchronization and inertial response in the APL is the approach typically encountered in the literature [16], and will here be referred to as *integrated GFM*. To overcome the described risk for instability present in these approaches, the cascaded structure for the converter's active-power controller displayed in Fig. 5 is proposed here. The PI-based APL tracks the active-power reference and synchronizes with the grid, and generates the angle for the converter virtual back EMF. To avoid the previously described problem, the bandwidth of the APL has to be relatively high, so that its inertial contribution is negligible.

The inertia response P_{H} is instead calculated by the IEL and added onto the APL's power reference P_{set}. This is similar to the approach proposed in [18], where a PLL is used to provide an inertial response from a grid-following converter. The advantage of the proposed approach over other methods to provide RoCoF-proportional inertial response is that the frequency derivative is implicitly determined within the PLL. This replaces the noise-sensitive derivation step and means that the RoCoF estimate is immediately available, reducing delays in the converter's inertial response [18]. By generating the inertial response explicitly as a part of the power reference, it can be effectively limited, preventing the previously demonstrated instability. For this, the admissible converter power $S_{\mathrm{lim}} = \frac{V_{\mathrm{g}} S_{\mathrm{N}}}{V_{\mathrm{N}}}$ is estimated with the rated converter power S_{N} and rated voltage V_{N}. It is used together with the reactive power injected by the converter, Q, to calculate the active-power limit, $P_{\mathrm{lim}} = (S_{\mathrm{lim}}^2 - Q^2)^{1/2}$, which is then applied to the active-power reference P_{ref}.

In contrast to the proposed solution, the inertial response from an actual or virtual synchronous machine is not achieved by varying the power reference, but is a natural reaction to a frequency transient while mechanical torque or power reference, respectively, are held constant. Due to that it is nontrivial in these control designs to limit the active power without compromising the loop's synchronization task. Separating the inertia from the APL as in the proposed cascaded controller gives on the other hand the possibility to prevent the current from exceeding its rated value by limiting the inertial power, which in turn avoids the triggering of the current limiter in Fig. 1. Generating the inertial response through the APL power setpoint comes furthermore with the advantage that the presented IEL can be used with any sufficiently fast APL, and can be even employed in grid-following converters to provide inertial response. Even though it is based on a PLL structure, the IEL does only provide inertia emulation, while the APL is exclusively responsible for active-power reference tracking and in a GFM for synchronization with the grid.

The other parts of the controller shown in Fig. 1 are tuned according to the method presented in [17]. While the active-power controller generates the virtual back EMF angle, its magnitude is determined by the voltage controller, here consisting of a simple integrator. The virtual admittance (VA) is used for calculation of the reference current input to the current controller. Thanks to its resistive-inductive nature, the VA provides reference-current filtering (through X_{v}) and damping (through R_{v}); furthermore, it helps in preserving the converter's dynamic performance under varying grid strengths by reducing the impact of the grid impedance on the total impedance variation [19][2]. The current references generated by the VA are limited with a circular current limitation and finally fed to the vector-current controller.

A. Active-power loop tuning

The APL employed in this paper is based on a PI-regulator. The adopted controller is tuned using a loop shaping approach with active damping. The active-power transfer from the converter to the grid neglecting resistances is given by the two port equation (2), which can be applied here due to the

[2]The virtual reactance is selected in the range of typical SM output reactance [20], while the virtual resistance is chosen to provide a small time constant for the dc-current offset originated from the large virtual reactance.

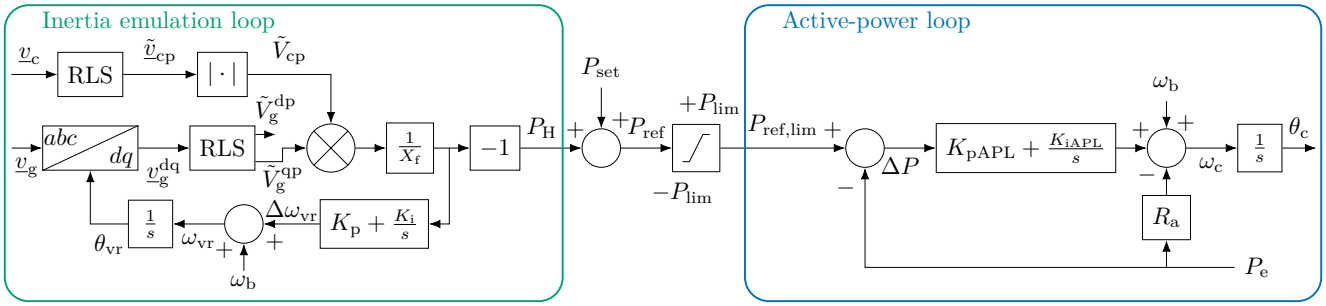

Fig. 5. Proposed cascaded structure for the active-power controller of GFM converters.

relatively slow speed of APLs, allowing to use quasi-steady state equations. To tune the controller properly, the equation is formulated with regard to the measurable PCC voltage instead of the Thévenin source, with $\delta = \theta_{\mathrm{EMF}} - \theta_{\mathrm{g}}$. Linearizing this equation for small angle differences, and formulating the transfer function for a change in the converter angle with a constant grid voltage phase angle gives the plant model for the controller design as

$$G_\theta(s) = \frac{\Delta P}{\Delta\theta_{\mathrm{EMF}}} = \frac{V_{\mathrm{EMF}} V_{\mathrm{g}}}{X_{\mathrm{V}}} = P_{\mathrm{vmax}}. \tag{5}$$

The linearized system model corresponds to a PI-controller controlling an integrator, which will result in a zero in the closed-loop transfer function and a pronounced overshoot in the step response. To remove this overshoot, the active damping term displayed in Fig. 5 is introduced. This is similar to the approach typically used for vector current controllers (e.g. as suggested in [21]) and results in the transfer function from the output of the PI-regulator to the injected active power

$$G_\omega(s) = \frac{\Delta P}{\Delta\omega_{\mathrm{c}}} = \frac{1}{R_{\mathrm{a}}} \frac{R_{\mathrm{a}} P_{\mathrm{vmax}}}{s + R_{\mathrm{a}} P_{\mathrm{vmax}}}, \tag{6}$$

which corresponds to a first-order system with the bandwidth $\alpha_\omega = R_{\mathrm{a}} P_{\mathrm{vmax}}$. As suggested in [21], this bandwidth is selected to match the desired control-loop bandwidth α_{PC}, resulting in

$$R_{\mathrm{a}} = \alpha_{\mathrm{PC}} / P_{\mathrm{vmax}}. \tag{7}$$

The closed-loop transfer function from the reference to the actual active power then becomes

$$G_{\mathrm{PC}}(s) = \frac{K_{\mathrm{pAPL}} s + K_{\mathrm{iAPL}}}{s^2 P_{\mathrm{vmax}}^{-1} + (K_{\mathrm{pAPL}} + R_{\mathrm{a}}) s + K_{\mathrm{iAPL}}}. \tag{8}$$

A proper selection of the loop's gains reduces the system order to one:

$$G_{\mathrm{PC}}(s) = \frac{\alpha_{\mathrm{PC}} s + \alpha_{\mathrm{PC}}^2}{s^2 + 2\alpha_{\mathrm{PC}} s + \alpha_{\mathrm{PC}}^2} = \frac{\alpha_{\mathrm{PC}}}{s + \alpha_{\mathrm{PC}}}, \quad \text{with} \tag{9}$$

$$K_{\mathrm{pAPL}} = R_{\mathrm{a}} = \frac{\alpha_{\mathrm{PC}}}{P_{\mathrm{vmax}}} \quad \text{and} \quad K_{\mathrm{iAPL}} = \frac{\alpha_{\mathrm{PC}}^2}{P_{\mathrm{vmax}}} = \alpha_{\mathrm{PC}} R_{\mathrm{a}}.$$

To keep in line with the proposed solution and limit the amount of inertia in the active-power loop, α_{PC} should be selected as high as feasible. As reported in [22], there exist grid code requirements limiting the APL bandwidth to 5 Hz, which corresponds to an inertia constant of approximately 0.32 s.

B. Inertia-emulation loop tuning

The IEL is tuned to behave equivalent in terms of inertial power contribution to a synchronous machine (SM). The IEL's output is the pure inertial response P_{H}, which is equivalent to a lossless synchronous condenser (SC), where the mechanical power $P_{\mathrm{m}} = 0$. The fundamental idea is that both SC and IEL track the phase angle of the grid voltage with a given speed, which corresponds to their inertia.

The relation between a change in rotor speed of the SM and an active-power imbalance is given by the swing equation:

$$2H \frac{\mathrm{d}\omega_{\mathrm{r}}}{\mathrm{d}t} = P_{\mathrm{m}} - P_{\mathrm{e}} - K_{\mathrm{d}}(\omega_{\mathrm{r}} - \omega_{\mathrm{s}}). \tag{10}$$

Here, H denotes the inertia constant in seconds, ω_{r} is the angular rotor frequency, ω_{g} the angular frequency of the grid voltage, P_{e} the electrical power injected to the grid and K_{d} the damping coefficient of the machine, with all quantities but H in pu. For a SM operating in a stable steady-state operating point, electrical and mechanical power must be equal. During a grid disturbance, the power imbalance in such a machine will be its inertial response $P_{\mathrm{H}} = P_{\mathrm{m}} - P_{\mathrm{e}}$. Laplace-transforming and rearranging yields

$$\omega_{\mathrm{r}} s = \frac{-P_{\mathrm{H}}}{2H} - \frac{K_{\mathrm{d}}}{2H}(\omega_{\mathrm{r}} - \omega_{\mathrm{s}}). \tag{11}$$

As the mechanical time constants are much higher than the electrical, the SM's electrical power P_{e} can be expressed in quasi-steady state as in (2), neglecting the resistances. Assuming a dq-coordinate frame that is aligned with the machine's back EMF results in

$$P_{\mathrm{e}} = \frac{V_{\mathrm{EMF}} V_{\mathrm{s}}}{X} \sin(\theta_{\mathrm{r}} - \theta_{\mathrm{s}}) = -\frac{V_{\mathrm{EMF}}}{X} V_{\mathrm{s}}^{\mathrm{q}}, \tag{12}$$

where $V_{\mathrm{s}}^{\mathrm{q}}$ denotes the source voltage q-component, and X the sum of reactances between the back EMF and source voltage. In the SC case with $P_{\mathrm{m}} = 0$, back EMF and grid voltage are aligned with each other in steady state and $V_{\mathrm{s}}^{\mathrm{q}}$ is zero. A change in the grid voltage phase angle would result in a misalignment of the voltages and an active power $P_{\mathrm{H}} = P_{\mathrm{e}}$.

For small angle differences, this can be linearized as

$$P_{\mathrm{H}} = \frac{V_{\mathrm{EMF}} V_{\mathrm{s}}}{X}(\theta_{\mathrm{r}} - \theta_{\mathrm{s}}) = \frac{V_{\mathrm{EMF}} V_{\mathrm{s}}}{X s}(\omega_{\mathrm{r}} - \omega_{\mathrm{g}}), \tag{13}$$

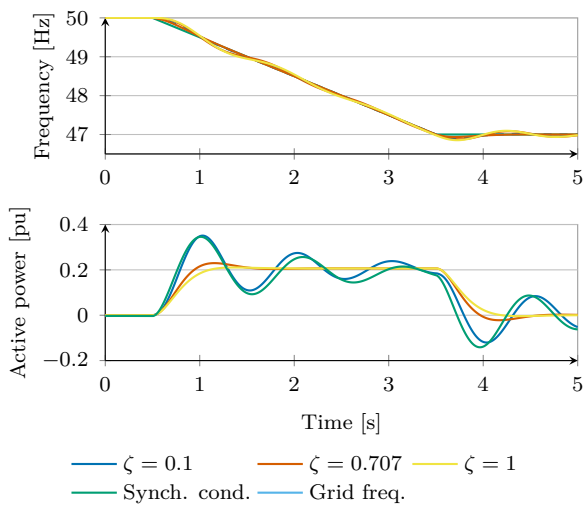

Fig. 6. Comparison with synchronous condenser and impact of the damping ratio on rise time and overshoot.

using the angular frequency and phase angle relationships

$$\theta_{\mathrm{r}} s = \omega_{\mathrm{r}} \qquad \text{and} \qquad \theta_{\mathrm{s}} s = \omega_{\mathrm{s}}. \tag{14}$$

In most cases the additional power and consequently angle difference due to inertial response is small, and the linearization creates only negligible deviations. Using the previous equation to rearrange (11) with the SM maximum transferable active power $P_{\mathrm{smax}} = \frac{V_{\mathrm{EMF}} V_{\mathrm{s}}}{X}$ results in

$$\omega_{\mathrm{r}} s = -\left(\frac{K_{\mathrm{d}}}{2HP_{\mathrm{smax}}} s + \frac{1}{2H}\right) P_{\mathrm{H}}. \tag{15}$$

Equivalent behaviour can be established for the IEL. If the emulated inertial-power reference P_{H} is chosen as the input to the IEL's PI-regulator, the derivative of the loop's internal frequency is determined as

$$\omega_{\mathrm{vr}} s = -(K_{\mathrm{p}} s + K_{\mathrm{i}}) P_{\mathrm{H}}, \tag{16}$$

where ω_{vr} is the loop's frequency estimate and K_{p} and K_{i} the proportional and integral gain, respectively. P_{H} is given by

$$P_{\mathrm{H}} = -\frac{V_{\mathrm{c}}}{X_{\mathrm{f}}} V_{\mathrm{g}}^{\mathrm{q}}, \tag{17}$$

with the PCC voltage q-component $V_{\mathrm{g}}^{\mathrm{q}}$ in the coordinate system aligned with the IEL angle θ_{vr}, and the filter reactance X_{f}. This equation is the two-port equation formulated with the converter terminal and PCC voltage. The virtual back EMF is replaced with the converter terminal voltage because the virtual resistance can take values that are too high to be neglected, making the use of the simplified two-port equation inaccurate. The Thévenin source voltage $\underline{V}_{\mathrm{s}}$ is replaced with the PCC voltage because the latter can be directly measured. The tracking behaviour of SM and IEL given in (11) and (16), respectively, can be related to each other to establish equivalent behavior with the following tuning:

$$K_{\mathrm{i}} = \frac{\omega_{\mathrm{b}}}{2H}, \quad K_{\mathrm{p}} = \frac{\omega_{\mathrm{b}} K_{\mathrm{d}}}{2HP_{\mathrm{max}}}, \quad \text{with} \quad P_{\mathrm{max}} = \frac{V_{\mathrm{c}} V_{\mathrm{g}}}{X_{\mathrm{f}}}. \tag{18}$$

This formulation assumes all quantities in the IEL are in pu with the exception of virtual angular frequency ω_{vr} and virtual rotor angle θ_{vr}, which is why the base angular frequency ω_{b} appears in both expressions. Thus, the integral gain of the IEL directly relates to the inertia constant of the SM behavior to be reproduced, while the proportional gain represents the damping. To receive an accurate replication of the desired inertial response it is advisable to substract the inertia constant remaining in the APL from the inertia constant used for the IEL so that the cumulative effect is as required.

C. Selection of damping

As mentioned above, the proportional gain relates to the damping of the inertial response from the IEL. The relation in (18) determines K_{p} if a specific SM damping coefficient is to be reproduced. In a SM, damping is linked to physical properties such as friction and typically associated with losses. In consequence, SMs are usually poorly dampened. In the IEL, the damping does not imply any losses, which means it becomes an additional degree of freedom. Increased damping comes however with the downside of a slower response.

In the previous section was established that inertial response relates to tracking changes in the grid voltage angle with a specific speed. This tracking speed is determined by the IEL closed loop transfer function, given as

$$G_{\mathrm{IEL}}(s) = \frac{\Delta\theta_{\mathrm{vr}}}{\Delta\theta_{\mathrm{g}}} = \frac{P_{\mathrm{max}}(K_{\mathrm{p}} s + K_{\mathrm{i}})}{s^2 + P_{\mathrm{max}} K_{\mathrm{p}} s + P_{\mathrm{max}} K_{\mathrm{i}}}, \tag{19}$$

employing the small angle linearization

$$\Delta\theta_{\mathrm{g}} = \frac{1}{V_{\mathrm{g}}} \Delta V_{\mathrm{g}}^{\mathrm{q}}. \tag{20}$$

This is a damped second order response with a zero,

$$G_{\mathrm{IEL}}(s) = \frac{2\zeta\omega_{\mathrm{n}} s + \omega_{\mathrm{n}}^2}{s^2 + 2\zeta\omega_{\mathrm{n}} s + \omega_{\mathrm{n}}^2}, \quad \text{where} \tag{21}$$

$$\omega_{\mathrm{n}} = \sqrt{\frac{\omega_{\mathrm{b}} P_{\mathrm{max}}}{2H}}, \quad \text{and} \quad \zeta = \sqrt{\frac{\omega_{\mathrm{b}}}{2HP_{\mathrm{max}}}} K_{\mathrm{d}}$$

using (18), which allows to determine the proportional gain based on the damping ratio as

$$K_{\mathrm{p}} = \zeta \sqrt{\frac{2\omega_{\mathrm{b}}}{HP_{\mathrm{max}}}}. \tag{22}$$

The effect of different damping ratios is shown in the results from time-domain simulations in Fig. 6. For this study case, the frequency of the voltage source is reduced with $1\,\mathrm{Hz/s}$ from $50\,\mathrm{Hz}$ to $47\,\mathrm{Hz}$, while the steady-state active-power reference is set to $P_{\mathrm{set}} = 0\,\mathrm{pu}$. The inertia constant is selected as $H = 4.68\,\mathrm{s}$, which together with the inertial contribution from the APL results in a total inertia constant of $5\,\mathrm{s}$, meaning that the frequency disturbance should result in an inertial response of $0.2\,\mathrm{pu}$. The figure demonstrates that the proposed controller is able to reproduce the behavior of a synchronous machine with good accuracy. The chosen approach to combine a fast APL with a change in the power reference causes a minor delay when compared to the physics based response

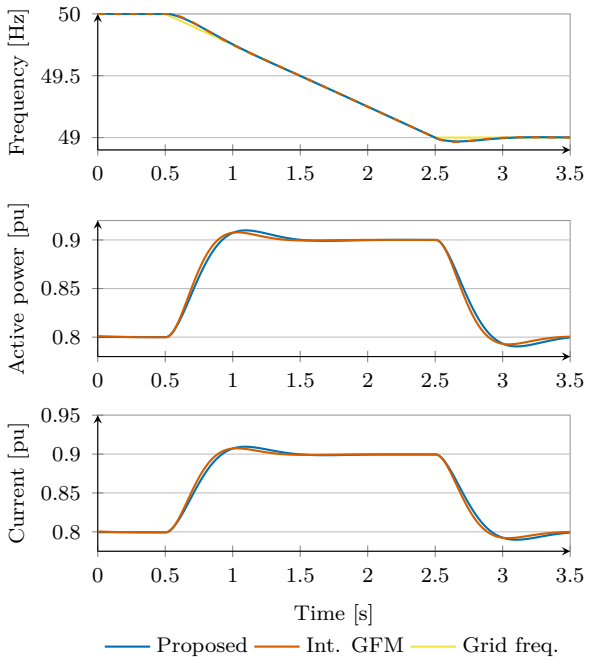

Fig. 7. Dynamic response of GFM converter to the smaller simulated frequency disturbance (0.5 Hz/s), not causing current saturation.

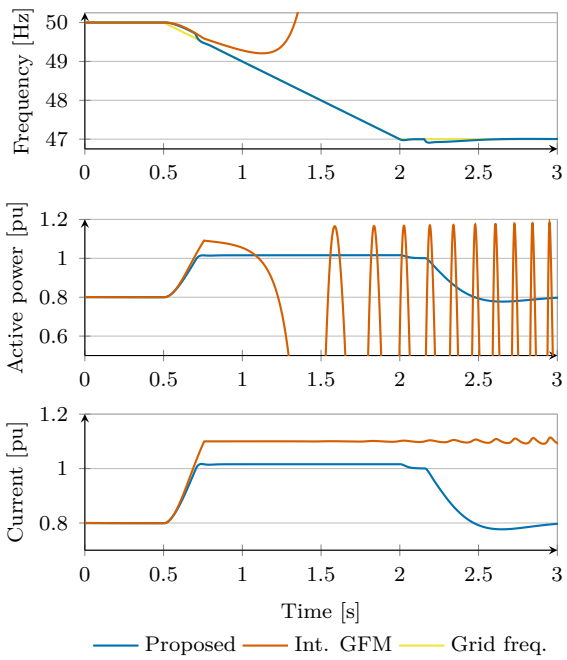

Fig. 8. Dynamic response of GFM converter to the larger simulated frequency disturbance (2 Hz/s), causing current saturation.

of the SM. It can also be seen that the low damping of the SM causes a challenging behavior. As the IEL damping can be freely adapted without any losses, a response without overshoot ($\zeta = 1$) can be selected. To reduce the rise time, a damping ratio of $\zeta = 0.707$ is suggested as a compromise between speed and damping of the inertial response.

D. Sequence separation and harmonic filtering

Unbalanced conditions or operation under distorted grid voltages impact the IEL and result in an unsteady inertial-power reference. To avoid this, a sequence separation is applied to the PCC and converter terminal voltages as shown in Fig. 5. For this paper, the recursive least square (RLS) based method from [23] is implemented in dq-coordinates. The transfer functions resulting from transforming the state-space model presented in [23] into dq-coordinates is

$$G_{\mathrm{RLSp}}(s) = \frac{\tilde{v}_{\mathrm{p}}^{\mathrm{dq}}}{v^{\mathrm{dq}}} = \frac{(\omega\xi - \mathrm{j}\omega\frac{\xi^2}{2})s + \omega^2\xi^2 + 2\mathrm{j}\omega^2\xi}{s^2 + (2\omega\xi + 2\mathrm{j}\omega)s + \omega^2\xi^2 + 2\mathrm{j}\omega^2\xi} \tag{23}$$

$$G_{\mathrm{RLSn}}(s) = \frac{\tilde{v}_{\mathrm{n}}^{\mathrm{dq}}}{v^{\mathrm{dq}}} = \frac{(\omega\xi + \mathrm{j}\omega\frac{\xi^2}{2})s}{s^2 + (2\omega\xi + 2\mathrm{j}\omega)s + \omega^2\xi^2 + 2\mathrm{j}\omega^2\xi}, \tag{24}$$

where $\tilde{v}_{\mathrm{p}}^{\mathrm{dq}}$ and $\tilde{v}_{\mathrm{n}}^{\mathrm{dq}}$ are the voltage dq-vector positive and negative sequence estimates, ω is the grid frequency[3] and ξ is the estimator's relative bandwidth. The RLS-algorithm provides not only sequence separation, but also effective harmonic filtering [23].

TABLE I
SYSTEM AND CONTROL PARAMETERS

System parameters		Control parameters	
S_{N}	1 kVA	L_{v1}	0.35 pu
V_{N}	100 V	R_{v1}	0.235 pu
ω_{b}	314.16 rad/s	α_{pc}	2π 5 rad/s
L_{f}	0.15 pu	H	4.68 s
R_{f}	0.015 pu	ζ	0.707
SCR	3	ξ	0.9 pu

IV. Simulation Results

The effectiveness of the proposed solution is validated by time-domain simulations of an average model of the grid-connected converter system shown in Fig. 1. The first case study compares the cascaded controller suggested here with an *integrated GFM* design for two frequency disturbances with different RoCoF, demonstrating both equivalence for operation below the active-power limit as well as the effectiveness of the suggested solution for ensuring robust operation in current saturation. In the next part, the effect of the RLS sequence separation is demonstrated, both in terms of added delay as well as the ability for unbalanced operation. Finally, operation under distorted grid voltage conditions is shown. The system and controller parameters used in the simulations are given in Table I. The over-current limit of the converter is set to 1.1 pu, S_{N} is 1.0 pu and a circular current limiter is used to limit the current reference.

A. Comparison with integrated GFM

The proposed cascaded power controller is compared to the integrated GFM control [6], which is tuned to the same inertia

[3]Here a fixed grid frequency is assumed and $\omega = \omega_{\mathrm{b}}$, but as shown in [23] a frequency adaptation can be used as well.

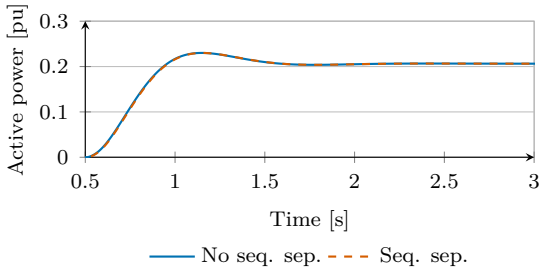

Fig. 9. Delay introduced to the inertial response due to the inclusion of the RLS sequence estimation.

constant, by simulating two disturbances. In both cases the PCC-voltage is controlled by the converter to $1.0\,\mathrm{pu}$, with an active-power reference of $P_{\mathrm{set}} = 0.8\,\mathrm{pu}$. The first study case is a frequency reduction of the infinite voltage source, ω_{s}, from $50.0\,\mathrm{Hz}$ to $49.0\,\mathrm{Hz}$ at a rate of $0.5\,\mathrm{Hz/s}$, while in the second case the frequency is varied with $2.0\,\mathrm{Hz/s}$ to a minimum of $47.0\,\mathrm{Hz}$. As shown in Fig. 7, in case of the smaller frequency disturbance the inertial power response from the two control structures is practically equal, demonstrating that an equivalent response can be achieved with the proposed design. The internal converter frequencies ω_{c} shown in the top plot are following the declining grid frequency closely. The active-power response exhibits a small delay for the cascaded controller, as in this case the inertial response is coming not from within the APL, but as a change in the power reference.

For the larger frequency disturbance shown in Fig. 8, synchronization is lost when the virtual inertia is provided directly in the APL and consequently the current limiter is saturated (integrated GFM control, red curves). The converter control with the proposed cascaded structure (blue curves) on the other hand is able to limit the current close to its rated value and keep synchronism with the grid. The active power exceeds the limit imposed on P_{ref} ($1\,\mathrm{pu}$), because despite of its high bandwidth the APL still contributes some inertia. Still, the converter current can be effectively limited to close to $1\,\mathrm{pu}$ without saturating the circular current limitation. It can also be noted that the inertial response continues for approximately $200\,\mathrm{ms}$ after the frequency transient has finished. This is due to the fact that the unlimited inertial response reference from the IEL is $0.4\,\mathrm{pu}$, but the response is limited at $0.2\,\mathrm{pu}$. The unlimited inertial response reference starts to decrease from the moment the transient ends, e.g. as in Fig. 7, but due to the limitation this becomes not visible before it has reduced to less than $0.2\,\mathrm{pu}$. This effect could be minimized by including an anti-windup, which increases the IEL bandwidth based on the saturation of the power reference limiter.

It has even been verified through simulations that there is no notable difference between the cascaded controller's and an integrated GFM's reaction to a grid voltage phase angle jump, apart from the cascaded controller's ability to prevent instability.

B. Unbalanced operation and harmonic filtering

The addition of the RLS-based sequence separation causes a small delay to the generated inertial response signal. As

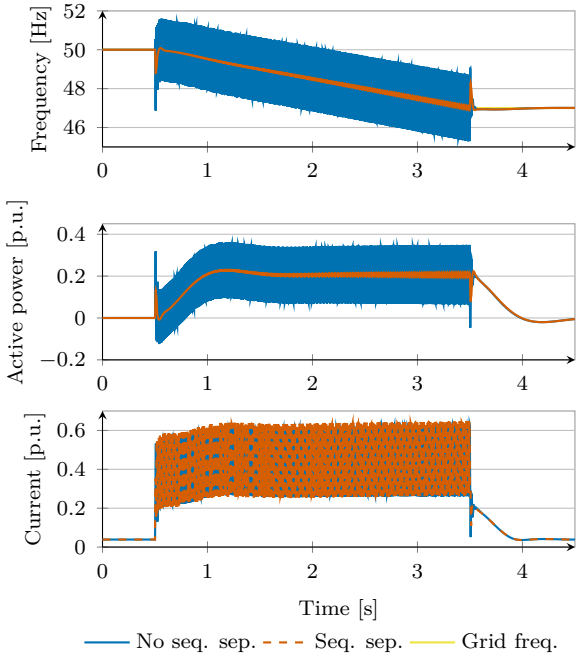

Fig. 10. IEL performance without and with sequence separation during an unbalanced voltage dip.

demonstrated in Fig. 9, this delay is only minimal. A more detailed analysis shows that the delay is around $5\,\mathrm{ms}$ and has therefore a neglectable impact on the inertial timescale. To demonstrate the necessity of sequence separation, additionally to the frequency transient a single-phase voltage dip is applied and the results are presented in Fig. 10. Without the sequence separation (blue curve), the negative sequence causes a $100\,\mathrm{Hz}$-oscillation in the dq-voltage vector, which is transferred into the voltage q-component and consequently inertial-power reference. The red curve shows the results including the sequence separation, and in this case the inertial-power reference is free from harmonic components. The only exception are transient oscillations at the beginning and end of the fault, which are caused by the time needed for the RLS to correctly estimate the sequence components. In Fig. 11, a 5^{th} and 7^{th} harmonic of $0.05\,\mathrm{pu}$ magnitude each are added to the source voltage. Even though the RLS is not tuned explicitely to remove these harmonic components, it can be seen that the majority of harmonic content is removed by the RLS and APL, both of which have a low-pass characteristic. This shows that a sequence separation is necessary, that the suggested method has a neglegible impact on the speed of the inertial response and that it effectively rejects oscillations due to unbalanced conditions and harmonic components. It has been verified with simulations that the RLS does not impact the robustness of the proposed approach negatively.

V. Conclusions

This paper demonstrates that grid frequency disturbances can cause instability in inertia-providing GFM converters, and that the existing strategies to manipulate the power reference during current saturation are ineffective in this case. To

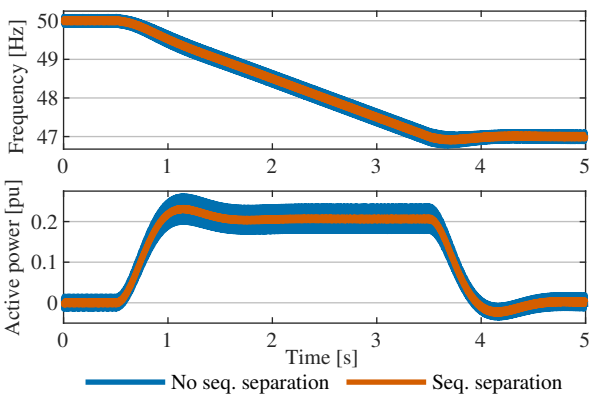

Fig. 11. IEL performance without and with sequence separation under the presence of voltage harmonics.

solve the problem of loss of synchronism due to a slow active-power loop exposed to current limitation, a cascaded power controller consisting of an IEL and a fast active-power controller is proposed. This approach effectively decouples the control elements responsible for provision of inertia and synchronization to the grid, resulting in a robust behavior even during frequency transients. The structure of the IEL is presented along with simulation results verifying that the proposed approach maintains a stable operation even during major disturbances. Future work on the proposed controller is necessary to investigate the stability limits of the proposed approach and improvements to its large disturbance robustness, as well as lab verification of the presented results.

REFERENCES

[1] J. Matevosyan *et al.*, "Grid-Forming Inverters: Are They the Key for High Renewable Penetration?" *IEEE Power and Energy Magazine*, vol. 17, no. 6, Nov. 2019.

[2] L. Huang, L. Zhang, H. Xin, Z. Wang, and D. Gan, "Current limiting leads to virtual power angle synchronous instability of droop-controlled converters," in *2016 IEEE Power and Energy Society General Meeting (PESGM)*, Jul. 2016.

[3] H. Lin, C. Jia, J. M. Guerrero, and J. C. Vasquez, "Angle Stability Analysis for Voltage-Controlled Converters," *IEEE Transactions on Industrial Electronics*, vol. 64, no. 8, Aug. 2017.

[4] T. Qoria *et al.*, "Critical Clearing Time Determination and Enhancement of Grid-Forming Converters Embedding Virtual Impedance as Current Limitation Algorithm," *IEEE Journal of Emerging and Selected Topics in Power Electronics*, vol. 8, no. 2, Jun. 2020.

[5] X. Wang *et al.*, "Grid-Synchronization Stability of Converter-Based Resources—An Overview," *IEEE Open Journal of Industry Applications*, vol. 1, 2020.

[6] M. G. Taul, X. Wang, P. Davari, and F. Blaabjerg, "Current Limiting Control With Enhanced Dynamics of Grid-Forming Converters During Fault Conditions," *IEEE Journal of Emerging and Selected Topics in Power Electronics*, vol. 8, no. 2, Jun. 2020.

[7] E. Rokrok, T. Qoria, A. Bruyere, B. Francois, and X. Guillaud, "Transient Stability Assessment and Enhancement of Grid-Forming Converters Embedding Current Reference Saturation as Current Limiting Strategy," *IEEE Transactions on Power Systems*, 2021.

[8] Y. Geng, L. Zhu, X. Song, K. Wang, and X. Li, "A Modified Droop Control for Grid-Connected Inverters With Improved Stability in the Fluctuation of Grid Frequency and Voltage Magnitude," *IEEE Access*, vol. 7, 2019.

[9] L. Xiong, X. Liu, D. Zhang, and Y. Liu, "Rapid Power Compensation-Based Frequency Response Strategy for Low-Inertia Power Systems," *IEEE Journal of Emerging and Selected Topics in Power Electronics*, vol. 9, no. 4, Aug. 2021.

[10] L. Huang *et al.*, "An Adaptive Inertia Control to Improve Stability of Virtual Synchronous Machines Under Various Power Grid Strength," in *2019 IEEE Power Energy Society General Meeting (PESGM)*, Aug. 2019.

[11] Z.-l. Li, J. Hu, and K. W. Chan, "A New Current Limiting and Overload Protection Strategy for Droop-Controlled Voltage-Source Converters in Islanded AC Microgrids Under Grid Faulted Conditions," in *2020 IEEE Energy Conversion Congress and Exposition (ECCE)*, Oct. 2020.

[12] L. Zhang, L. Harnefors, and H. Nee, "Power-Synchronization Control of Grid-Connected Voltage-Source Converters," *IEEE Transactions on Power Systems*, vol. 25, no. 2, May 2010.

[13] A. Gkountaras, S. Dieckerhoff, and T. Sezi, "Evaluation of current limiting methods for grid forming inverters in medium voltage microgrids," in *2015 IEEE Energy Conversion Congress and Exposition (ECCE)*, Sep. 2015.

[14] J. Rocabert, A. Luna, F. Blaabjerg, and P. Rodríguez, "Control of Power Converters in AC Microgrids," *IEEE Transactions on Power Electronics*, vol. 27, no. 11, Nov. 2012.

[15] ENTSO-E, "High Penetration of Power Electronic Interfaced Power Sources and the Potential Contribution of Grid Forming Converters," 2020.

[16] R. Rosso, X. Wang, M. Liserre, X. Lu, and S. Engelken, "Grid-Forming Converters: Control Approaches, Grid-Synchronization, and Future Trends — A Review," *IEEE Open Journal of Industry Applications*, vol. 2, 2021.

[17] A. Narula, M. Bongiorno, M. Beza, and P. Chen, "Tuning and evaluation of grid-forming converters for grid-support," in *2021 23rd European Conference on Power Electronics and Applications (EPE'21 ECCE Europe)*, Sep. 2021.

[18] M. van Wesenbeeck, S. de Haan, P. Varela, and K. Visscher, "Grid tied converter with virtual kinetic storage," in *2009 IEEE Bucharest PowerTech*, Jun. 2009.

[19] A. Narula, M. Bongiorno, and M. Beza, "Comparison of Grid-Forming Converter Control Strategies," in *2021 IEEE Energy Conversion Congress and Exposition (ECCE)*, Oct. 2021.

[20] P. Rodriguez, I. Candela, C. Citro, J. Rocabert, and A. Luna, "Control of grid-connected power converters based on a virtual admittance control loop," in *2013 15th European Conference on Power Electronics and Applications (EPE)*, Sep. 2013.

[21] L. Harnefors, *Control of Variable Speed Drives*. Sep. 2002.

[22] P. Imgart, M. Beza, M. Bongiorno, and J. R. Svensson, "An Overview of Grid-Connection Requirements for Converters and Their Impact on Grid-Forming Control," *EPE'22 ECCE Europe (accepted for publication)*, 2022.

[23] M. Beza and M. Bongiorno, "Application of Recursive Least Squares Algorithm With Variable Forgetting Factor for Frequency Component Estimation in a Generic Input Signal," *IEEE Transactions on Industry Applications*, vol. 50, no. 2, Mar. 2014.